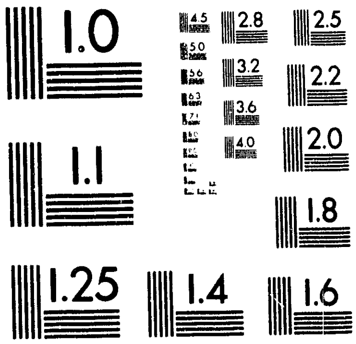
1.0
1.1
1.25
1.4
1.6
1.8
2.0
2.2
2.5
2.8
3.2
3.6
4.0
4.5
5.0
5.6
6.3

1 of 1

Conf-9305210--3

Fast Ion Behavior During Neutral Beam Injection in ATF*

M. R. Wade, C. E. Thomas, S. C. Aceto,** R. J. Colchin, J. A. Rome, A. C. England, and R. H. Fowler

Oak Ridge National Laboratory, Oak Ridge, Tennessee, 37831, USA

In stellarators, single-particle confinement properties can be more complex than in their tokamak counterparts. Fast-ion behavior in tokamaks has been well characterized through an abundance of measurements on various devices and in general has been shown to be consistent with classical slowing-down theory [1–5], although anomalous ion behavior has been observed during intense beam injection in ISX-B [6], during fishbone instabilities in PDX [7], and in experiments onTFR [8]. In contrast, fast-ion behavior in stellarators is not as well established experimentally with the primary experiments to date focusing on near-perpendicular or perpendicular neutral beam injection (NBI) on the Wendelstein 7-A stellarator [9] and Heliotron-E [10]. This paper addresses fast-ion confinement properties in a large-aspect-ratio, moderate-shear stellarator, the Advanced Toroidal Facility (ATF),during tangential NBI.

The primary data used in this study are the experimentally measured energy spectra of charge-exchange neutrals escaping from the plasma, using a two-dimensional scanning neutral particle analyzer (NPA). This diagnostic method (charge-exchange neutral analysis) is well established, having been used on several devices since the early 1970's [11-15]. Various aspects of fast-ion behavior are investigated by comparing these data with computed theoretical spectra based on energetic-ion distributions derived from the fast-ion Fokker-Planck equation [16]. Ion orbits are studied by computer orbit following, by the computation of J^* surfaces, and by Monte Carlo calculations.

Experimental Arrangement

Figure 1 shows a plan view of the ATF torsatron (R_0 = 2.10 m, $\bar{a}$ = 0.28 m) and the relative locations of the two neutral beam injectors and the NPA. The injectors are aimed tangentially, 0.13 m inside the magnetic axis, to minimize scrape-off of the beams on the vacuum vessel walls [17]. The opposing orientation of the injectors allows

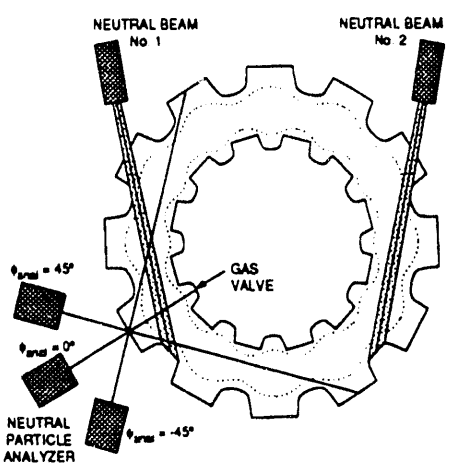

FIG. 1. Plan view of ATF showing the relative locations of the two neutral beam injectors and the NPA. Three possible orientations of the NPA are shown.

* Research sponsored by the Office of Fusion Energy, U.S. Department of Energy, under contract DE-AC05-84OR21400 with Martin Marietta Energy Systems, Inc.

** Rensselaer Polytechnic Institute, Troy, NY 12181, USA.

DISCLAIMER

balanced injection with no net momentum input or net beam-driven current. For the experiments discussed here, fast hydrogen neutrals are injected at energies up to 35 keV; the delivered power is distributed among the three energy components in the ratio 70:20:10.

Plasmas in ATF are initiated by 400 kW of 53.2-GHz electron cyclotron heating (ECH), providing second-harmonic heating at the standard on-axis magnetic field, $B_0 = 0.95$ T, and fundamental heating for $B_0 = 1.90$ T. Because absorption of the ECH-launched wave decreases dramatically in regions where the characteristic plasma frequency ($\omega_{pi} \sim n_e^{1/2}$) is approximately the same as the wave frequency, an effective cutoff density exists such that for densities above this limit, the ECH power absorption is no longer adequate to prevent thermal collapse. One would expect this cutoff density to be at the point where the central electron density reaches a level such that $\omega_{cut} > \omega_{ech}$. For an ECH-launched wave of 53.2 GHz in extra-ordinary mode at second harmonic with $B_0 = 0.95$ T, the expected cutoff density is $n_e = 1.7 \times 10^{19}$ m^{-3}. However, data from ATF suggests that the effective cutoff density is actually less than this level at $n_e^{cut} \equiv 0.8 \times 10^{19}$ m^{-3}. The primary consequence of this phenomenon is that during NBI large shine-through and charge-exchange losses are present. Furthermore, at the onset of NBI, the plasma density typically increases rapidly due to beam fueling and quickly exceeds the ECH cutoff density. Since the coupled beam power does not rise quickly enough to account for this sudden loss in ECH power, the plasma is subject to a thermal collapse because of insufficient heating to maintain the electron temperature above the radiative collapse limit.

Fast-ion spectra are measured by a mass- and energy-analyzing spectrometer [18]. This analyzer has two mass columns (allowing for simultaneous measurements of H and D), each having 39 fully instrumented energy channels with an effective energy range of $0.5 \le A(\text{amu}) \cdot E$ (keV) ≤ 600. The NPA is mounted on a carriage that allows it to be moved horizontally and vertically. When the analyzer is scanned horizontally, its viewing angle can be changed from perpendicular to tangential (in either direction) to the magnetic field. The vertical scanning capability allows the analyzer to scan from below to above the plasma column in ATF. For most of the data presented, the vertical viewing angle is $\theta_{anal} = 0^\circ$ (i.e., viewing along the horizontal midplane of ATF). The NPA hardware, the associated data acquisition and control systems, and calibration of the system are described in more detail in Refs. [18–19].

Observations

Operating experience on ATF has shown that the available operating space (in terms of plasma electron density) during NBI is limited. Quasi–steady state plasmas have been attained in two situations: low density (below the ECH cutoff density, $\bar{n}_e \le 7.5 \times 10^{18}$ m^{-3}) and extremely high density ($\bar{n}_e \ge 8 \times 10^{19}$ m^{-3}). For intermediate densities, the plasma either undergoes a thermal collapse (loss of all thermal energy) or has peculiar transient behavior.

A typical tangential fast–ion slowing-down energy spectra measured by the NPA in a low-density discharge is shown in Fig. 2. The tangency radius of the viewing angle , $\phi_{anal} = 45^\circ$, roughly corresponds to the tangency radius of the

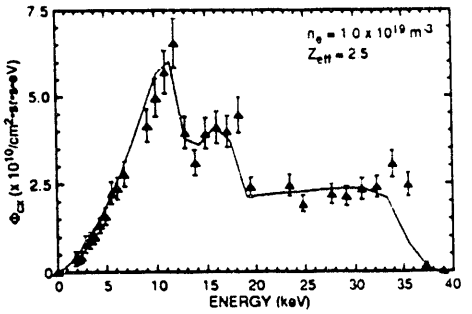

FIG. 2. Tangential fast-ion energy spectrum measured by the NPA in a low-density discharge. The prediction of the Fokker-Planck code is shown as a solid line.

beam. In low-density discharges in which the electron density continuously rises from the onset of NBI until a thermal collapse occurs, the three energy peaks become less well defined and the magnitude of the flux decreases slightly as the density increases (as is the case for the data of Fig. 2). Both of these observations are consistent with a decrease in the charge-exchange loss –an indication that the coupling of the fast ions to the plasma is improving throughout the discharge. Also shown in Fig. 2 is the spectrum calculated using the Fokker–Planck code, assuming a global particle confinement time τ_p = 20 msec and an average edge neutral energy E_{edge} = 5 eV. These parameters are consistent with those used in other studies of thermal ion confinement in ATF. At the time at which this spectrum was taken, the central electron and ion temperatures were approximately 250 eV and $Z_{eff} \approx 2.0$. The excellent agreement between the measured and the computed spectrum in Fig. 2 suggests that the thermalization process of tangentially injected ions in ATF is well described by classical processes. Excellent agreement between measurements and Fokker–Planck calculations has also been obtained for analyzer viewing angles as small as ϕ_{anal} = 20°.

Perpendicular slowing-down spectra were also measured in these types of discharges. In the low-density discharges, the measured spectra have a peculiar "hole" in the spectra typically near E = 4 keV (see Fig. 3). Similar

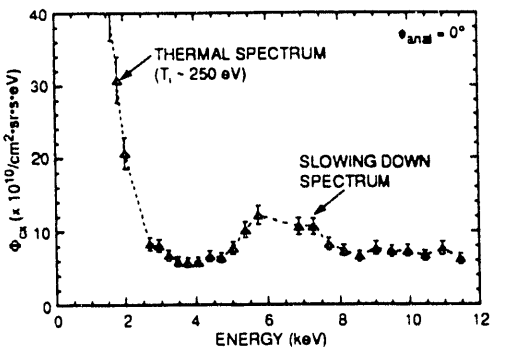

FIG. 3. Perpendicular (ϕ_{anal} = 0°) energy spectrum measured by the NPA during a low-density discharge exhibiting a "hole" at approximately 4 keV. B_0 = 0.95 T.

spectra (with the "hole" occurring at the same energy) have been obtained during operation at B_o = 1.9 T, indicating that the measured effect is not dependent on the magnetic field. From classical slowing-down arguments, one would expect the thermal distribution (energies less than 3 keV) to merge smoothly with the energetic-ion distribution. This is clearly not the case in Fig. 3, where the measured spectrum exhibits either a "hole" near 4 keV or a "bump" near 6 keV. Since possible mechanisms that could cause an enhancement in confinement at 6 keV are not known, it is assumed that the measured spectra are due to a deterioration in confinement of 4-keV particles.

This "hole" is likely due to an effect associated with the radial electric field in ATF. In a stellarator, the radial electric field plays an important role in the

confinement of low-energy helically trapped ions. If the electric field is of the right magnitude such that the poloidal drift due to $\vec{E}_r \times \vec{B}$ drift cancels the poloidal ∇B drift due to the helical windings, the helically trapped ion will drift vertically out of the device because of the uncompensated toroidal curvature drift. This effect has a resonant feature in energy, since the ∇B drift is a function of particle energy and the $\vec{E}_r \times \vec{B}$ drift is not. In ATF, this resonance occurs at approximately the energy $4.0e|\Phi_0|$, where Φ_0 is the magnitude of the central electrostatic potential (assuming a parabolic potential profile). For this so-called helical resonance to occur, Φ_0 must be negative with respect to the potential at the plasma boundary (i.e., the radial electric field is directed inward). The electrostatic potential profile measured by a heavy-ion beam probe [20] in ATF during NBI is shown in Fig. 4, and is in the correct direction

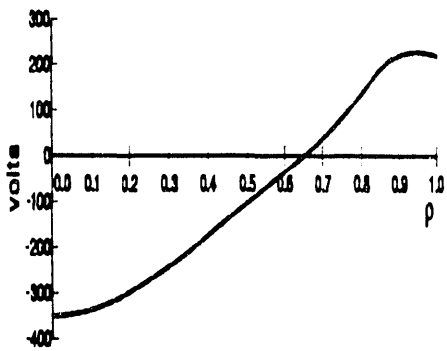

FIG. 4. Potential measured by a heavy-ion-beam-probe as a function of ρ = r/a during NBI.

for this resonance to occur. There also is experimental evidence from both Wendelstein W7-A and Heliotron-E that the potential becomes negative during NBI [21,22], even though both of these devices use perpendicular injection, where large, direct ion losses are expected. More recent results from CHS using tangential NBI also have shown that the radial electric field is directed inward (indicating a negative central potential) [23]. This suggests that the helical resonance is the likely source of the "hole" in the measured NPA spectra in ATF. A similar "hole" was observed in Heliotron-E and was attributed to this helical resonance effect [24].

Fast Ion Orbit and Monte Carlo Calculations

The ATF magnetic field configuration was primarily designed to reach the second stability region of confinement. It is therefore of interest to check this configuration for its ability to contain fast–ion orbits. It is found that loss regions exist which can play a role in fast–ion slowing down.

Following individual ion orbits by computer can be quite time–consuming. Fortunately, an adiabatic invariant J^* can be derived [25]. Contours of constant J^* define the ion trapping regions . An example of this type of calculation is shown in Fig. 5 (a), where the three branches of J^* along with the trapping boundary are shown for the standard ATF magnetic configuration (assuming $e\Phi = 0$ and $\lambda = \mu B_{min} / qE = 0.59$) It is evident that the degree to which the helically trapped particles (and in general, all particles) are confined is critically dependent on the value of λ, or equivalently the pitch angle $v_{\parallel}/v$ of the particle of interest.

The accuracy of this approach is evident from a comparison of orbits that have been computed from the equations of motion with the corresponding J^* contours. This comparison is shown in Fig. 5(b). Note that the motion predicted by the constant J^* contours is the motion of the guiding center in the untrapped region and the motion of the banana center in the trapped region. Therefore, details of the exact orbits are not provided by this method. This can be

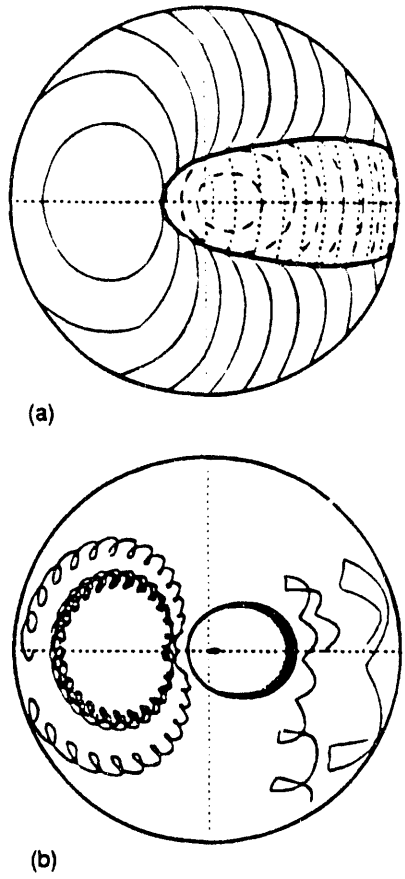

FIG. 5. (a) Contours of constant J^* plotted in Boozer coordinates for E = 5 keV ions. The J^* contours corresponding to trapped particles are shown as the solid lines, while the J^* contours for untrapped particles are shown as the dashed (copassing) and dotted (counterpassing) lines. The bold solid curve represents the trapping boundary for the particular choice of λ. (b) Ion orbits computed using an orbit–following code with the same E and λ.

seen in Fig. 5(b), where, although the computed orbits have fairly large excursions from the predicted J^* contour, the guiding centers of the orbits tend to follow the same path. The orbits on the right-hand side of Fig. 5(b) are examples of transitional particles that are predicted fairly accurately from the constant J^* approach. These particles start on the horizontal midplane as locally copassing particles (i.e., they follow a constant J^*_{co} contour). As an injected fast ion slows down, it initially loses energy, which causes a "shrinking" of its orbit size, but its pitch angle (velocity vectors) remains fairly constant. After reaching the critical energy, $E_{crit} \approx 14.8\ T_e$, its pitch angle (or equivalently λ) begins to increase.

As these particles reach the trapping boundary [bold, solid line in Fig. 5(a)], a transition must occur where the particle continues its orbit on a constant J^*_{ctr} contour or a constant J^*_{trap} contour. In this case, the particles are reflected at the boundary and follow J^*_{ctr} contours back through the locally passing region. As they encounter the trapping boundary the next time, the particles become helically trapped and subsequently follow the appropriate J^*_{trap} contour out of the confinement region. By examining contour plots similar to these, the entire orbit topology for a fixed configuration can be determined. This reduces the task of assessing single-particle confinement characteristics of a given configuration to a manageable level.

Fig. 6 shows the result of incorporating the potential of Fig. 4 into the

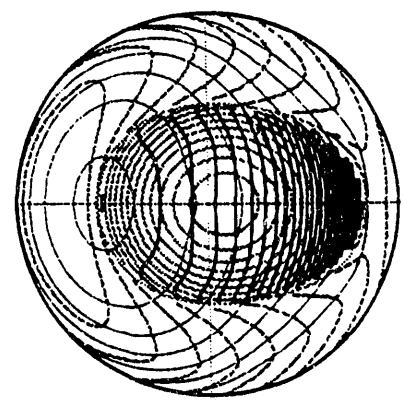

FIG. 6. J^* contours in Boozer coordinates for E = 4 keV copassing (light solid lines), counterpassing (dark solid lines), and trapped (dashed lines) ions.

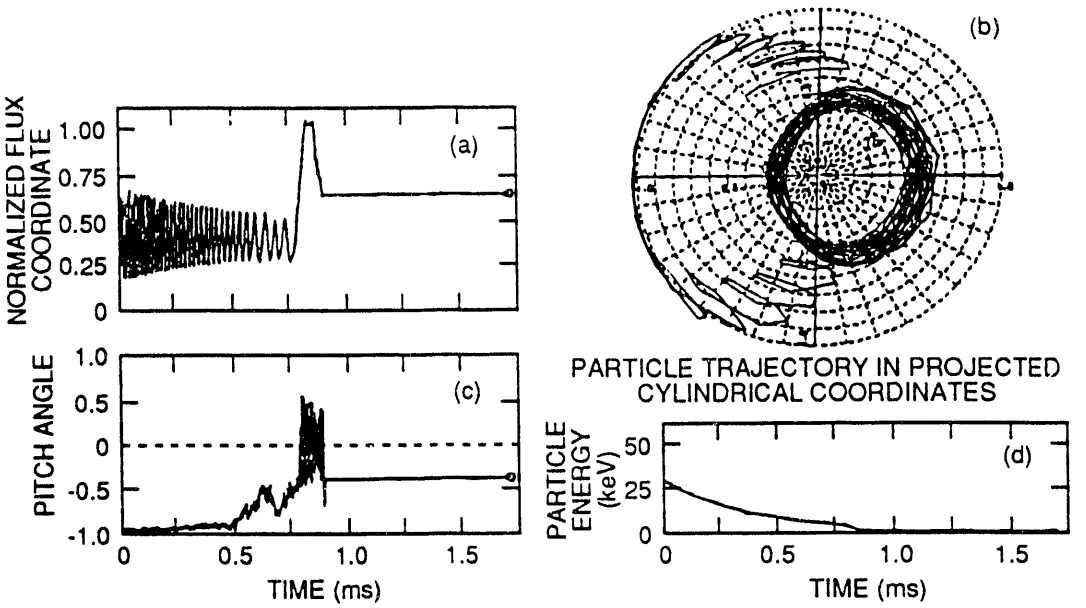

FIG. 7. Monte Carlo calculation for a tangentially injected ion in ATF: (a) the normalized flux coordinate vs time, (b) representation of the particle trajectory projected in Boozer coordinates, (c) the pitch angle of the particle vs time, and (d) the energy of the particle vs time.

calculation of the J^* contours. Note that the ions generally have the same types of loss orbits as those in Fig. 5.

Monte Carlo calculations were performed to simulate this slowing–down process, using the DESORBS [26] code. Fig. 7 shows a sample Monte Carlo simulation for the standard ATF magnetic field configuration (R_0 = 2.08 m, B_0 = 0.95 T). Charge-exchange has been turned off in this particular calculation so that the particle's motion can be tracked to the thermalization of the particle. This particular particle is born (ionized) near the center of the plasma with an initial pitch angle near $v_{\|}/v = -1$, which is copassing in this case. Initially, as the particle slows down, its pitch angle remains fairly constant because the particle's energy is well above the critical energy and momentum transfer is dominated by collisions with the plasma electrons. The projection of the initial orbit is simply a circle whose center is slightly shifted outside the magnetic axis. However, as the particle slows down further and its energy approaches the critical energy ($E_{crit} \approx 10$ keV in this case), the injected ion starts to suffer substantial pitch–angle scattering as collisions with ions become more prevalent. Eventually, the particle suffers enough pitch-angle scattering that it crosses the trapping boundary and becomes helically trapped. The helically trapped orbit then carries the particle out to the plasma boundary. In this case, with charge-exchange turned off, the particle reenters the plasma, since its orbit does not intersect the ATF vacuum vessel.

The lack of a connecting path between confined passing and trapped particles constitutes a problem for confinemenent of 3-5 keV fast ions. However, as far as heating efficiency is concerned, this particle loss is severe only when the average energy at which the injected particles reach the trapping boundary is a

substantial fraction of the injection energy.

Summary

Fast–ion confinement behavior has been studied both experimentally, by neutral particle analysis, and computationally, by means of Fokker-Plank, Monte Carlo, and orbit codes. Ions injected into low–density ($\bar{n}_e \sim 10^{19}$ m^{-3}) plasmas are found to slow down classically until they undergo pitch–angle scattering. Loss cones exist which act to prevent the beam particles from reaching thermal energy, as evidenced by a "hole" observed in the distribution function.

References

[1] CORDY, J. G., et al., Nucl. Fusion **15** (1975) 441.
[2] GOLDSTON, R. J., Nucl. Fusion **15** (1975) 651.
[3] EQUIPE TFR, Nucl. Fusion **18** (1978) 1271.
[4] KAITA, R., et al., Nucl. Fusion **25** (1985) 939.
[5] HEIDBRINK, W. W., KIM, J., GROEBNER, R., Nucl. Fusion **28** (1988) 1897.
[6] CARNEVALI, A., et al., Nucl. Fusion **28** (1988) 951.
[7] GOLDSTON, R. J., et al., Nucl. Fusion **27** (1987) 921.
[8] EQUIPE TFR, in *Plasma Physics and Controlled Fusion Research* 1986 (Proc. 11th Int. Conf., Kyoto, 1986), Vol. 1 (IAEA, Vienna, 1987), p. 179.
[9] W VII-A TEAM, et al., in *Plasma Physics and Controlled Fusion Research* 1984 (Proc. 10th Int. Conf., London, 1984), Vol. 2 (IAEA, Vienna, 1985), p. 371.
[10] UO, K. et al., in *Plasma Physics and Controlled Fusion Research* 1984 (Proc. 10th Int. Conf., London, 1984), Vol. 2 (IAEA, Vienna, 1985), p. 383.
[11] ARTSIMOVICH, L. A., et al., Sov. Phys. JETP **34** (1972) 306.
[12] DAVIS, S. L., MUELLER, D., KEANE, C. J., Rev. Sci. Instrum. **54** (1983) 315.
[13] ROQUEMORE, A. L., et al., Rev. Sci. Instrum. **56** (1985) 1120.
[14] HAYASHI, K., HASHIMOTO, K., YAMATO, H., Rev. Sci. Instrum. **56** (1985) 359.
[15] HEIDBRINK, W. W., Rev. Sci. Instrum. **59** (1988) 1679.
[16] CORDY, J. G., CORE, W. G., Phys. Fluids **17** (1974) 1626.
[17] MORRIS, R. N., et al., Nucl. Tech./Fusion **12** (1987) 281.
[18] WADE, M. R., et al., Rev. Sci. Instrum. **61** (1990) 3202.
[19] WADE. M.R., "*An Experimental Study of Ion Behavior in the Advanced Toroidal Facility*," Ph.D. thesis, Georgia Institute of Technology, 1991.
[20] ACETO, S. C., et al., in *Controlled Fusion and Plasma Physics* (Proc. 18th EPS Conf., Berlin, 1991), Vol. 15C, Part II (1991), *p.* 161.
[21] WOBIG, H., et al., in *Plasma Physics and Controlled Fusion Research* 1986 (Proc. 11th Int. Conf., Kyoto, 1986), Vol. 2, (IAEA, Vienna, 1987), p. 369.
[22] KONDO, K., et al., Rev. Sci. Instrum. **59** (1988) 1533.
[23] IDA, K., et al., Phys. Fluids B **3** (1991) 515.
[24] HANITANI, K., et al., in *Controlled Fusion and Plasma Physics* (Proc. 14th EPS Conf., Madrid, 1987), Vol. 11D, Part I (1987), *p.* 396.
[25] CARY, J. R., HEDRICK, C. L., TOLLIVER, J. S., Phys. Fluids **31** (1988) 1586.
[26] FOWLER, R. H., MORRIS, R. N., ROME, J. A., HANITANI, K., Nucl. Fusion **30** (1990) 997.

DATE
FILMED
11/4/93
END